Accepted Manuscript

Title: A Highly Selective Cr/ZrO_2 Catalyst for the Reverse Water-Gas Shift Reaction Prepared from Simulated Cr-containing Wastewater by a Photocatalytic Deposition Process with ZrO_2

Author: Yang Tao Yingming Zhu Changjun Liu Hairong Yue Junyi Ji Shaojun Yuan Wei Jiang Bin Liang

PII: S2213-3437(18)30653-5
DOI: https://doi.org/doi:10.1016/j.jece.2018.10.043
Reference: JECE 2728

To appear in:

Received date: 26-5-2018
Revised date: 13-9-2018
Accepted date: 17-10-2018

Please cite this article as: Y. Tao, Y. Zhu, C. Liu, H. Yue, J. Ji, S. Yuan, W. Jiang, B. Liang, A Highly Selective Cr/ZrO_2 Catalyst for the Reverse Water-Gas Shift Reaction Prepared from Simulated Cr-containing Wastewater by a Photocatalytic Deposition Process with ZrO_2, *Journal of Environmental Chemical Engineering* (2018), https://doi.org/10.1016/j.jece.2018.10.043

[Title Page]

A Highly Selective Cr/ZrO_2 Catalyst for the Reverse Water-Gas Shift Reaction Prepared from Simulated Cr-containing Wastewater by a Photocatalytic Deposition Process with ZrO_2

Yang Tao[a], Yingming Zhu[b], Changjun Liu[a], Hairong Yue[a], Junyi Ji[a], Shaojun Yuan[a], Wei Jiang[a,1], Bin Liang[a,b]

[a]Multi-Phase Mass Transfer and Reaction Engineering Laboratory, School of Chemical Engineering, Sichuan University, Chengdu, 610065, China.

[b]Institute of New Energy and Low-carbon Technology, Sichuan University, Chengdu, 610065, China.

[1] Corresponding author. Tel.: +86-28-85990133; fax: +86-28-85460556.
E-mail address: weijiang@scu.edu.cn

A Highly Selective Cr/ZrO_2 Catalyst for the Reverse Water-Gas Shift Reaction Prepared from Cr-containing Wastewater by a Photocatalytic Deposition Process with ZrO_2

Yang Tao[a], Yingming Zhu[b], Changjun Liu[a], Hairong Yue[a], Junyi Ji[a], Shaojun Yuan[a], Wei Jiang[a,2], Bin Liang[a,b]

[a]Multi-Phase Mass Transfer and Reaction Engineering Laboratory, School of Chemical Engineering, Sichuan University, Chengdu, 610065, China.

[b]Institute of New Energy and Low-carbon Technology, Sichuan University, Chengdu, 610065, China.

Abstract

Here, we report the preparation of a Cr/ZrO_2 composite catalyst for the reverse water-gas shift reaction (RWGS) that shows excellent low-temperature CO_2 conversion and 100% CO selectivity. The catalyst was prepared from Cr-containing wastewater by photoreduction. Zirconia was used as a wide bandgap photocatalyst to photoreduce Cr(VI) under UV irradiation and immobilize the Cr species on the catalyst surface, resulting in a high dispersion. The results show that the obtained 1wt%Cr/ZrO_2 can catalyze the RWGS to reach the thermodynamic limit at 600 ℃. The CO yield at

[2] Corresponding author. Tel.: +86-28-85990133; fax: +86-28-85460556.
E-mail address: weijiang@scu.edu.cn

600 °C with photoreduced Cr/ZrO_2 after calcination, 38.34%, is significantly higher than that of the catalyst prepared by impregnation. Metal hydrides were determined to be the key intermediates in the RWGS reaction with Cr/ZrO_2 as the catalyst, and the cyclic conversion between Cr(VI) and Cr(III) caused by the hydrogen reduction and CO_2 oxidation improves the catalytic activity. This study provides a strategy to acquire a promising RWGS catalyst for CO_2 emission reduction and utilization and an attractive method to treat Cr-containing wastewater.

Keywords: Reverse water-gas shift reaction; Cr/ZrO_2 catalyst; Photoreduction deposition; Cr-containing wastewater; *In situ* Raman

1. Introduction

Carbon dioxide hydrogenation is an effective strategy for CO_2 emission reduction and utilization[1], and the reverse water-gas shift reaction (RWGS) is an attractive and promising route[2] for this process with industrial value. CO_2 is typically inert but can be activated and converted into valuable CO with low hydrogen consumption in the RWGS. The CO can be used for further production with value-added products such as methanol[3] in the CAMERE (Carbon Dioxide Hydrogenation to Form Methanol via a Reverse-Water-Gas-Shift Reaction) process and alkenes[4] in alkane oxidative dehydrogenation.

As a typical endothermic reaction, the RWGS reaction enthalpy is 42.1 kJ mol^{-1}. Thus, the most favorable reaction conditions involve high temperatures and a high ratio of hydrogen to CO_2 for reaction conversion enhancement. However, the high reaction temperatures result in high energy consumption and rapid catalyst deactivation because of severe carbon deposition, as well as competitive methanation side reactions. A high hydrogen-to-carbon ratio increases the operating costs and makes it difficult to adjust the proper hydrogen-carbon ratio for follow-up production. Thus, the development of a catalyst with excellent low-temperature activity and good anti-coking capability with a low hydrogen-to-carbon ratio for the RWGS was investigated.

Currently, investigations into RWGS catalysts can be classified into two types: noble metal catalysts such as Pt[5], Au[6], Rh[7], and Pd[8] and non-noble-metal catalysts including Cu[9], Ni[10], Fe[11], Zn[3]and In[12]. The noble metal catalysts exhibit excellent CO_2 conversion at low temperatures, but the CO selectivity is relatively poor

and the cost is high. On the other hand, the non-noble-metal catalysts have unsatisfactory activities and selectivities at low temperatures, and coking is facile at high temperatures, although their cost is relatively low. Therefore, the development of a catalyst with the advantages of both types of catalysts, i.e., low cost, low-temperature CO_2 conversion, and high CO selectivity, is attractive.

Notably, Cr-containing catalysts have been widely used for the oxidative dehydrogenation of alkanes[13], which uses an RWGS process to eliminate the hydrogen generated from alkanes with CO_2. In these processes, Cr species can effectively promote the elimination of hydrogen dissociated from the C-H bonds of the alkane with CO_2 by means of the RWGS, promoting the generation of alkenes. Coke deposition can also be alleviated by carbon elimination with CO_2. These applications indicate that Cr species could be promising RWGS catalysts. However, the direct use of Cr-containing catalyst for RWGS is not often reported. Mamedov et al.[14] attempted to employ Catofin® (17wt%Cr/Al_2O_3), a commercial catalyst for propene production, as the low-temperature RWGS catalyst. The CO_2 conversion was 25.1% at 600 °C and atmospheric pressure with a 1:1 hydrogen-to-CO_2 molar ratio and a gas space hourly velocity (GSHV) of 254.8 h^{-1}. Sang-Woo Park et al.[15] used Cr_2O_3 as a carrier to load different active components to catalyze the RWGS, and ZnO/Cr_2O_3 was found to be the best catalyst. Thus, it is expected that Cr could be an effective active component for the RWGS, but its performance must be further improved.

Improving the dispersion of the active components is a useful method to improve the catalyst activity, and photocatalytic reduction deposition is a promising method to

achieve this. Theoretically, metal components can be photoreduced and deposited on the photocatalyst carrier surface as a single atom layer to achieve a high dispersion. However, current research into the photodeposition process has mainly focused on the loading of noble metal components such as Pt[16], Au[17], and Ag[18]. The photoreduction of Cr species with common photocatalysts such as TiO_2[19] and ZnO[20] only converts Cr(VI) into soluble Cr(III). No Cr species were immobilized on the photocatalyst surface to form a Cr-containing composite. This lack of success could be ascribed to the relatively low photoreducibility arising from the narrow bandgap of TiO_2 and ZnO. However, if the band gap of the photocatalyst is sufficiently large, soluble Cr can be reduced to insoluble Cr species such as Cr(0) and Cr_2O_3.

Zirconia is a relatively common and cheap photocatalyst with a wide bandgap. In addition, it is widely used as a catalyst and catalyst support in hydrogenation and dehydrogenation reactions. The band gap of zirconia is 5.0 eV[21], and the conduction band is 1.09 eV[21], which is larger than the redox potentials of the Cr(VI)/Cr(III) (1.36 eV) and Cr(III)/Cr(0) (-0.74 eV) couples. Thus, it is possible to obtain a Cr/ZrO_2 composite by photoreduction.

In this study, ZrO_2 was used as the carrier to reduce and load Cr species as active the components by photoreduction from a Cr-containing solution, thereby constructing a Cr/ZrO_2 composite. The catalytic performance of the obtained Cr/ZrO_2 composite for the RWGS was evaluated and compared with a catalyst prepared by an impregnation method. The catalytic mechanism of Cr/ZrO_2 for RWGS will also be explored to determine its advantages.

2. Experimental

2.1. Catalyst Preparation

ZrO_2 nanoparticles were prepared by a typical sol-gel method. The particle size of the ZrO_2 nanoparticles was less than 0.15 mm after screening with a 100-mesh sieve. Particles of this size were selected to eliminate inner diffusion effects. A 50 mg L^{-1} $K_2Cr_2O_7$ solution (Cr content) was used as the chromium source. A 500-W mercury lamp was employed as the UV light source. The photoreduction process was carried out in a 50-mL quartz tube with 20 mL $K_2Cr_2O_7$ solution, 100 mg ZrO_2, and 2 mL methanol as the hole scavenger. All materials were added to the tube simultaneously and placed in the dark for 40 min to reach adsorption equilibrium. Subsequently, the suspension was exposed to UV light for 4 h. The obtained by-product of photoreduction, Cr/ZrO_2, was separated centrifugally from the aqueous solution and dried by vacuum freeze drying without any further treatment. The final product is denoted U-Cr/ZrO_2.

As a comparison, the U-Cr/ZrO_2 sample after calcination in air at 650 °C for 2 h is denoted C-Cr/ZrO_2 and that after reduction at 500 °C with hydrogen for 2 h is denoted R-Cr/ZrO_2. Another comparative sample, I-Cr/ZrO_2, is that prepared by the volumetric impregnation method using chromium nitrate as the chromium source containing 1 wt% Cr followed by calcination at 650 °C for 2 h.

In addition, a simulated Catofin® catalyst (Cr/Al_2O_3) containing 17% Cr and prepared by a volumetric impregnation method was prepared as a comparison.

2.2 Catalyst Characterization

X-ray diffraction (XRD) measurements were carried out using glancing angle X-ray diffraction (X'Pert ProMPD, The Netherlands) with a Cu Kα 40 kV/40 mA X-ray source. The Brunauer–Emmett–Teller (BET) were carried out with Micromeritics Instrument 2460.Scanning electron microscopy (SEM) was carried out with a JSM-7500F field-emission scanning electron microscope (JEOL). Ultraviolet-visible Diffuse Reflectance Spectrum (UV-vis DRS) was acquired by using a UV−vis spectrophotometer (TU-1901, Ge Beijing Spectrometer, China) to acquire the band gap of samples. The chromium content in the ZrO_2 composite was determined by using inductively coupled plasma optical emission spectrometry (ICP-OES, Vista Axial, Varian). X-ray photoelectron spectroscopy (XPS) measurements were carried out on a Thermo Fisher Scientific ESCALAB 250XI with monochrome Al Kα ($h\nu$ = 1486.6 eV). Temperature programmed desorption (TPD) and reduction (TPR) were carried out on a Micromeritics Instrument Corporation Auto Chem II 2920 and Boynton Beach FL33426 of Quantachrome, respectively. In Situ Raman Tests was carried by DXR Microscope (Thermo Fisher) using an excitation wavelength of 455nm with a power of 6 mW. The dispersion of Cr species was detected by transmission electron microscopy (TEM) mapping with Tecnai G2 F20 of FEI. X-ray Fluorescence Spectrometer (XRF-1800, Shimadazu) was employed to determined Cr content loaded.

2.3 Catalytic Performance Evaluation

About 0.15 g of the catalyst was placed in a quartz tube with an inner diameter of 4 mm in a continuous-flow fixed-bed reactor. The reactant stream consisting of H_2, N_2

(employed as internal standard gas), and CO_2 (H_2: CO_2: N_2 = 1:1:0.2) was introduced into the reactor at a flow rate of 55 mL min^{-1} at atmospheric pressure after eliminating internal and external diffusion. The reaction temperature ranged between 400 and 800 °C. The products were analyzed by gas chromatography (Fuli Instruments, FL9790II) with a TDX-01 column connected to a thermal conductivity detector (TCD). The conversion of CO_2 and selectivity of CO or CH_4 are defined as:

$$X_{CO_2} = \frac{CO_{2(in)} - CO_{2(out)} \times \frac{N_{2(in)}}{N_{2(out)}}}{CO_{2(in)}} \times 100\%$$

$$S_{CO} = \frac{CO_{(out)} \times \frac{N_{2(in)}}{N_{2(out)}}}{CO_{(out)} \times \frac{N_{2(in)}}{N_{2(out)}} + CH_{4(out)} \times \frac{N_{2(in)}}{N_{2(out)}}} \times 100\%$$

$$S_{CH_4} = 1 - S_{CO}$$

Here, $CO_{2(in)}$ and $N_{2(in)}$ are the concentrations of CO_2 and N_2 at the inlet, respectively, and $N_{2(out)}$, $CO_{(out)}$, and $CH_{4(out)}$ are the concentrations of N_2, CO, and CH_4 at the outlet, respectively.

3. Results and Discussion

3.1 Photoreduction of a Cr(VI) Solution with ZrO_2

The total chromium removal rate is shown in **Fig. 1-a**. About 90% of the soluble Cr species in the water was eliminated within 60 min. After 240 min, the Cr(VI) in solution was considered to have been entirely eliminated because the residual Cr concentration was 0.0413 mg·L^{-1}, which meets the strictest standards for drinking water (0.05 mg·L^{-1}, as regulated by WHO). The Cr content on the ZrO_2 increased with increasing irradiation time, and the total amount of loaded Cr was in accordance with the amount

removed from the water, confirming the successful immobilization of the dissolved Cr species.

The photographs in **Fig. 1-a (I~IV)** show the color change of the solution and the ZrO_2 powder before and after photoreduction. The solution changes from yellow to colorless and transparent, and the ZrO_2 powder changes from white to light green, which visually confirms the removal of Cr(VI) from the solution and the capture of Cr by ZrO_2 in the photoreduction process. This result confirmed the success of Cr loading on the ZrO_2 surface, suggesting that this is a promising method to treat Cr(VI) wastewater by photoreduction.

3.2 Catalytic Performance of Cr/ZrO_2 for RWGS

The catalytic performance of the Cr/ZrO_2 obtained from the photoreduction process, U-Cr/ZrO_2, and the samples after reduction and calcination, denoted R-Cr/ZrO_2 and C-Cr/ZrO_2, were assessed for the RWGS, and the results are shown in **Fig. 1-b**. Pure Cr_2O_3 and ZrO_2, as well as 1wt%Cr/ZrO_2(I-Cr/ZrO_2) and 17wt%Cr/Al_2O_3 prepared by means of impregnation, were used for comparison, as shown in **Fig. 1-c**. Promisingly, the determined CO selectivities of all samples were 100% over the whole tested temperature range, although the CO_2 conversion of each sample varied. No by-products, such as methane, methanol, or coke, were detected, in accordance with previous reports, suggesting that only CO_2 conversion must be considered to assess the RWGS catalytic performance of the samples.

We found that the RWGS activities of the Cr/ZrO_2 catalysts are significantly higher than those of pure ZrO_2 and Cr_2O_3, as well as 17%Cr/Al_2O_3, although the latter three

can also catalyze the RWGS to some extent. A sharp CO_2 conversion increase was observed between 400 and 600 °C in all Cr/ZrO_2 catalysts, both photoreduced and impregnated. The performance of C-Cr/ZrO_2 is significantly higher than others including U-Cr/ZrO_2 and R-Cr/ZrO_2, reaching the maximum RWGS thermodynamic limit of 38.4% at 600 °C. In contrast, the CO_2 conversion of pure ZrO_2 and Cr_2O_3 increased slowly before 600 °C and then rose sharply after 600 °C. For 17%Cr/Al_2O_3, the CO_2 conversion increased proportionally with increasing temperature between 400 and 800 °C. This result suggests that photoreduced Cr/ZrO_2 has an excellent RWGS catalytic activity and thermal pre-treatment can further improve its performance.

The stability of C-Cr/ZrO_2 was assessed at 500 °C, 0.1 MPa, CO_2:H_2 = 1:1, and GHSV = 22000 mL g^{-1} h^{-1}). In this test, the system was intentionally shut down and restarted twice to evaluate the operational stability. The results of the continuous operations are shown in **Fig. 1-d,** demonstrating that there was only a slight loss in catalytic performance of C-Cr/ZrO_2 from 28% CO_2 conversion to 24% after 72 h continuous operation with two reaction halts at 500 °C. However, in a single cycle, the performance was stable. In conclusion, the service life of C-Cr/ZrO_2 is promising for future industrial applications.

3.3 Characterization of C-Cr/ZrO_2

To determine the mechanism resulting in the superb performance of C-Cr/ZrO_2, we investigated the morphology, structure, and components of the catalysts before and after use. I-Cr/ZrO_2 was used as a comparison sample.

The XRD analysis results are shown in **Fig. 2-a**, showing that only peaks characteristic of ZrO_2 (2θ = 28.199°, 31.486°, 50.377°, and 50.711°) were observed for all Cr/ZrO_2 samples, that is, pure monoclinic ZrO_2 at 28.199° and 31.486 and tetragonal ZrO_2 at 50.377° and 50.711°. No significant changes to the crystal structure were observed for fresh and used C-Cr/ZrO_2 and I-Cr/ZrO_2, indicating that the performance difference between these catalysts is not due to the structure of the photocatalyst carriers. Furthermore, it can be reasonably assumed that the Cr species on the ZrO_2 surface are amorphous and highly disperse because no peaks corresponding to Cr species were observed.

The Brunauer–Emmett–Teller (BET) results for the five samples are shown in **Table 1**. The specific surface area of ZrO_2 decreased from 62 to 45 m^2 g^{-1} after photoreduction and calcination and further to 18 m^2 g^{-1} after use. The impregnated samples, I-Cr/ZrO_2, had relatively greater surface areas and pore volumes than C-Cr/ZrO_2 at the same stage but similar pore diameters. However, after use, the specific surface area and pore volume of I-Cr/ZrO_2 and C-Cr/ZrO_2 both decreased to the same extent, although their pore sizes increased synchronously. Thus, the effect of surface area and porosity on the catalytic performance difference between C-Cr/ZrO_2 and I-Cr/ZrO_2 can be excluded because the activity of the former was always better than that of the latter.

The UV-vis diffuse reflectance spectroscopy (DRS) results of I-Cr/ZrO_2, C-Cr/ZrO_2, U-Cr/ZrO_2, pure ZrO_2, and pure Cr_2O_3 are compared in **Fig. 2-b.** The peak at 228 nm is assigned to ZrO_2 and the peaks at 384, 450, and 600 nm are assigned to Cr_2O_3[22] in agreement with the results for pure ZrO_2 and pure Cr_2O_3, respectively. The determined

absorption edge of pure ZrO_2 and U-Cr/ZrO_2 were both 287 nm, corresponding to a band gap of 4.32eV. However, peaks at 384 and 600 nm were observed for of U-Cr/ZrO_2, and these peaks are assigned to Cr_2O_3 with octahedral symmetry, confirming the existence of Cr_2O_3 after photoreduction. However, for I-Cr/ZrO_2 and C-Cr/ZrO_2, the absorption edge shifted to 364 and 375 nm, which might be due to changes in the particle sizes and interactions between Cr species and ZrO_2 carriers during calcination. The peak at 384 nm assigned to Cr_2O_3 was observed for both samples. However, for C-Cr/ZrO_2, the peak at 600 nm disappeared, and the intensity of the peak at 384 nm was reduced compared with that of U-Cr/ZrO_2, confirming the transformation of Cr species after calcination.

XPS analysis of Cr on the photoreduced Cr/ZrO_2 was carried out to identify its transformation after calcination and after use. As shown in **Fig. 3-a**, the co-existence of Cr(0) and Cr(III) in fresh U-Cr/ZrO_2 was confirmed because the peaks at 583.50 and 574.20 eV, assigned to Cr(0)[23], and at 586.30 and 576.81 eV, assigned to Cr(III) of Cr_2O_3[24], were observed simultaneously. This fact confirmed that the photoreduced product of Cr(VI) with ZrO_2 was a multivalent Cr mixture. After calcination in air at 650 °C, new peaks at 588.2 and 578.3 eV, ascribed to Cr(VI) of CrO_3[25], were detected, but those of Cr(0) disappeared while those of Cr(III) remained. About 31.2% Cr(VI) was generated on C-Cr/ZrO_2 after calcination. However, after use, only Cr(III) was observed. Comparatively, the XPS results of I-Cr/ZrO_2 before and after use are shown in **Fig. 3-b**. Only characteristic peaks of Cr(III) of Cr_2O_3 were detected in both

samples. This result indicates that the valence transformation of Cr was the key factor for the improvement in the catalytic performance of C-Cr/ZrO_2.

The SEM results in **Figs. 4a–4d** show the morphology of I-Cr/ZrO_2 and C-Cr/ZrO_2 before and after use. The aggregation of grains on the surface of the large support particles can be seen. The size of the grains deposited on the C-Cr/ZrO_2 was significantly smaller than that on I-Cr/ZrO_2 at the same stage. The grain size also increased after use in both I-Cr/ZrO_2 and C-Cr/ZrO_2. The differences in morphology confirms the different dispersions of the two samples.

For further understanding the high dispersion of photoreduced Cr on ZrO2, a High-angle annular darkfield scanning transmission electron microscopy (HAADFSTEM) test of C-Cr/ZrO_2 was conducted and shown as Fig. 4e-4g. The wide distribution and uniform dispersion of Cr atoms marked in cyan on surface of ZrO_2 support can be observed. However, the relatively sparse distribution density of Cr element confirmed its limited amount, which was accordance to the assumption that photoreduced Cr elements immobilized on ZrO_2 surface with high dispersion and low toplimit. The XRF results determined was only about 0.35wt%, reaffirming the low content of Cr.

3.4 TPO and TPR Analysis

Because a change in the Cr valence is a possible factor resulting in the difference in catalytic performance between I-Cr/ZrO_2 and C-Cr/ZrO_2, TPO and TPR analysis were conducted to investigate the co-existence of different Cr species and possible interconversion between them.

As shown in **Fig. 5-a**, a significant oxidation peak at about 160 °C was detected in the TPO curve for U-Cr/ZrO_2. This narrow, sharp peak was ascribed to the oxidation of Cr(0) to Cr(III), although the oxidation of metallic Cr occurred at 300 °C. This activation of Cr(0) could be ascribed to its high dispersion. In addition, two small and smooth peaks at about 343 and 454 °C were detected, which were assigned to the partial oxidization of Cr(III) to Cr(VI) according to the XPS results. This result confirmed the valence change of the Cr species of U-Cr/ZrO_2 on calcination and indicates that Cr(III) can produce oxygen vacancies at relatively low temperatures.

Subsequently, H_2-TPR measurements were conducted on U-Cr/ZrO_2, I-Cr/ZrO_2, and C-Cr/ZrO_2, and the results are shown in **Fig. 5-b**. For U-Cr/ZrO_2, only one reduction peak at about 460 °C in the range of 25 to 800 °C was detected, which is ascribed to the reduction of Cr(III) to Cr(0)[26]. The activation of Cr(III) reaffirmed the high dispersion state of the Cr species because of the significant decrease in the Cr_2O_3 reduction temperature from 1200 °C as a pure substance to 460 °C in the composite[27]. However, for C-Cr/ZrO_2, peaks at 282 and 312 °C, assigned to the two forms of Cr(VI), were observed, which is in agreement with the TPO results. A peak at 445 °C assigned to the reduction of Cr(III) to Cr(0) was also observed. Thus, the above results reaffirm the co-existence of multivalent Cr species of photoreduced Cr/ZrO_2.

However, for I-Cr/ZrO_2, only a peak at 453 °C, assigned to the reduction of Cr(III) to Cr(0), was detected, confirming the existence of pure Cr_2O_3, which is in agreement with the XPS results. Notably, the reduction temperature of Cr(III) to Cr (0) of C-Cr/ZrO_2, 445 °C, is lower than those of U-Cr/ZrO_2 and I-Cr/ZrO_2. This result indicates

that the Cr(III) on C-Cr/ZrO_2 has a stronger association capability for hydrogen than in the other two catalysts, which indicates a better dehydrogenation ability.

3.5 CO_2-TPD and CO-TPD

The chemisorption state of the reactant CO_2 on the surface of ZrO_2, Cr_2O_3, C-Cr/ZrO_2, and I-Cr/ZrO_2 were determined by CO_2-TPD, and the results are shown in **Fig. 5-c.** The amount of chemically adsorbed CO_2 is listed in **Table 2.**

Two strong desorption peaks of pure ZrO_2 at 150 °C, assigned to the physical adsorption of CO_2, and a later desorption at 596 °C, which was ascribed to the acid-base interaction of CO_2 with the support, were observed. The strong CO_2 adsorption of ZrO_2 (317.66 μmoL g^{-1}) is disadvantageous for the dissociation of C=O bonds. However, for pure Cr_2O_3, only a weak peak at 412 °C was detected. This low CO_2 capacity (34.95 μmoL g^{-1}) is also unfavorable for the RWGS, although the low desorption temperature is favorable. This also explains the better RWGS catalytic activity of Cr_2O_3 than ZrO_2.

For the Cr-loaded samples, the peaks at 135 °C for I-Cr/ZrO_2 and at 141 °C for C-Cr/ZrO_2 are due to the physical adsorption of CO_2, but the peaks at 455 and 526 °C for I-Cr/ZrO_2 and at 471 and 524 °C for C-Cr/ZrO_2 are due to CO_2 chemisorption with a strong adsorption capacity. The shift in the CO_2 adsorption peaks of the two samples confirms the interaction between loaded Cr species and the ZrO_2 support, excluding the mechanical mixing of pure ZrO_2 and Cr_2O_3. The CO_2 chemical adsorption capacity of the composite was significantly enhanced after the immobilization of Cr species on the ZrO_2 surface, showing a slightly increased desorption temperature compared to that of

pure Cr_2O_3. The CO_2 adsorption capacity of C-Cr/ZrO_2 was the highest, suggesting that it has better CO_2 catalytic activity. This favorable improvement in the CO_2 chemisorption on Cr/ZrO_2 is beneficial for the RWGS reaction. Furthermore, a noteworthy fact is that the CO_2 adsorption peak area at 471 °C ascribed to the Cr_2O_3 component of C-Cr/ZrO_2 is significantly greater than that at 455 °C of I-Cr/ZrO_2, but the peak at 524 °C assigned to the ZrO_2 support of C-Cr/ZrO_2 is similar to that at 526 °C in I-Cr/ZrO_2. This result indicates the improved low-temperature CO_2 adsorption capacity and activity of C-Cr/ZrO_2 compared to I-Cr/ZrO_2.

The CO-TPD analysis of the four samples is shown in **Fig. 5-d,** and their CO chemical adsorption capacities are shown in **Table 2**. Only a desorption peak at 570 °C for ZrO_2 was detected, and the associated capacity is 101.54 μmoL g^{-1}. For pure Cr_2O_3, two extremely strong CO desorption peaks at 500 and 582 °C were detected. Although the first CO desorption temperature is relatively low, the adsorption capacity is high (843.10 μmoL g^{-1}), and the second desorption will worsen the Cr_2O_3 catalytic performance. However, after loading on the ZrO_2 surface, the CO desorption was weakened significantly. For I-Cr/ZrO_2, only a peak at 523 °C was detected, corresponding to a CO adsorption capacity of 331.41 μmoL g^{-1}. This significant weakening and shift in the CO adsorption peak could be ascribed to the interaction of the Cr_2O_3 and ZrO_2 carrier. For C-Cr/ZrO_2, the CO adsorption capacity was significantly reduced to 95.59 μmoL g^{-1} without an observable desorption peak. This reduction in CO adsorption means that the CO product can leave the catalyst surface

immediately after generation, effectively improving the catalytic performance of C-Cr/ZrO_2.

3.6 In Situ Raman Tests

Although the better activity of C-Cr/ZrO_2 can be explained by the TPD results, it is necessary to investigate the occurrence of the RWGS with C-Cr/ZrO_2 as a catalyst to obtain a deep understanding and further improvement. Thus, Raman analysis of ZrO_2, Cr_2O_3, and C-Cr/ZrO_2 was conducted, and the results are shown in **Fig. 6-a**. For pure ZrO_2, peaks at 212, 300, 325, 374, 466, 529, 550, 608, and 628 cm^{-1} belonging to the monoclinic phase and a peak at 256 cm^{-1} belonging to the tetragonal phase[28] were observed. For pure Cr_2O_3, only three low-intensity peaks at 295, 334, and 534 cm^{-1} were detected.

After loading the Cr on ZrO_2, the tetragonal ZrO_2 was covered by loaded Cr species and the peaks disappeared because of the relatively high photocatalytic activity of ZrO_2 as the support. However, the characteristic peaks of Cr_2O_3 were not observed, but these could be masked by the strong reflections of monoclinic ZrO_2. However, the slight shift in the peaks corresponding to monoclinic ZrO_2 confirm the interaction between the carrier and active components. New peaks at 862 and 1004 cm^{-1}, assigned to Cr-O-Cr bonds and the terminal Cr=O bond of polychromate, and at 1031 cm^{-1}, assigned to the terminal Cr=O bond of monochromate[29], were observed. Thus, the presence of Cr(VI) was reaffirmed.

In situ Raman analysis of the C-Cr/ZrO_2 sample was carried out by heating the sample to 400 °C in a nitrogen atmosphere and to 700 °C in the presence of a hydrogen

feed, and the results are shown in **Fig. 6-b**. The three new peaks at 862, 1004, and 1031 cm^{-1} vanished immediately after the introduction of H_2, confirming the reduction of Cr(IV) to Cr(III). However, two new peaks at 1350 and 1585 cm^{-1} appeared at the same time. Their intensity strengthened and position gradually shifted from 1350 to 1318 cm^{-1} and 1585 to 1568 cm^{-1} with increasing time and temperature. These two peaks arising after the introduction of H_2 could correspond to Zr-H and Cr-H hydride bonds, respectively. In addition, the corresponding peaks of ZrO_2 were enhanced at 400 °C. This enhancement after the introduction of hydrogen indicates the interactions between ZrO_2 and the reduced Cr(III) from Cr(VI) by hydrogen.

On cooling the sample from 700 to 36 °C in the presence of an N_2 and H_2 mixture, the In situ Raman results shown in **Fig. 6-c** exhibited a consecutive strengthening of the two new peaks corresponding to the Zr-H and Cr-H bonds. This result indicates that the hydrogenation of Zr and Cr increased with increasing reduction time despite the reduction temperature decreasing, which is beneficial for successive CO_2 hydrogenation in the RWGS. Another unexpected observation was the reappearance of peaks ascribed to Cr(VI) at 862, 1004, and 1031 cm^{-1} under a reductive atmosphere at 36 °C.

Subsequently, the sample was reheated from 36 to 400 °C after flushing with N_2, followed by refeeding H_2 into the system from 400 to 500 °C. As shown in **Fig. 6-d**, the peaks assigned to Cr-H and Zr-H, disappeared, and the peaks corresponding to Cr(VI) at 400 °C in N_2 increased. This fact confirms the role of hydrogen in forming an intermediate with metal hydrogen bonds. However, the corresponding peaks of metal

hydrides reappeared, and the Cr(VI) peaks disappeared again on the reintroduction of H_2.

H_2 was then replaced with CO_2 at 500 °C, and time-dependent in situ Raman analysis was carried out. The results are shown in **Fig. 7-a**. Then, H_2 was reintroduced into the CO_2 flux, and peaks corresponding to the hydrides (1335 and 1577 cm^{-1}) reappeared, and the peaks corresponding to Cr(VI) disappeared. Thus, it can be deduced that there is an interchange between Cr(IV) and hydrides on alternately feeding H_2 or CO_2.

Then, a new C-Cr/ZrO_2 sample was used to carry out the Raman analysis under N_2 and CO_2 atmospheres from room temperature to 600 °C to exclude the possible influence of the hydrogenated catalyst. The results in **Fig. 7-b** show the emergence of two peaks at 1368 and 1581 cm^{-1} at room temperature and their disappearance at 500 °C. These peaks arise from pure CO_2 and could be ascribed to the symmetric and asymmetric vibrations of C=O in the formates generated from the adsorbed CO_2[30]which are similar to the peaks assigned to the metal hydrides. The two new peaks should differ from the peaks ascribed to Cr-H at 1585 cm^{-1} and Zr-H at 1350 cm^{-1} although their shapes are similar and the peaks are close together. However, the two peaks of C=O in formates disappeared at temperatures beyond 500 °C. This instability made it possible to distinguish the characteristic peaks of hydrides and formates.

Then, the RWGS reaction with C-Cr/ZrO_2 was carried out at 400 °C by switching the feed to a mixture of H_2, CO_2, and N_2. In situ Raman results shown in **Fig. 7-c** show that the peaks corresponding to polychromate at 849 and 1007 cm^{-1} disappeared at 400 °C with the hydrogen feed, but the peak corresponding to monochromate at 1026

cm^{-1} only weakened with increasing temperature. This fact indicates that polychromate was easier to reduce than monochromate, implying that the possible hydrogen adsorption sites could be polychromate, thereby generating Cr-H intermediates. The peaks at 1354 and 1567 cm^{-1} were assigned to the hydrides because they were stable beyond 500 °C.

The in situ RWGS reaction with C-Cr/ZrO_2 was conducted continuously at 500 °C. The Raman results shown in **Fig. 7-d** show the disappearance of the Cr(VI) peaks and the strengthening of the hydride peaks at 1350 and 1585 cm^{-1} with increasing reaction time. Because the Cr-H bonds and Zr-H bonds are stable in this reaction, it can be determined that these two hydrides originating from the reduction of Cr(VI) by hydrogen are the key intermediates for the RWGS reaction with C-Cr/ZrO_2 as a catalyst.

The mechanism of the RWGS reaction with C-Cr/ZrO_2 as the catalyst was determined, as shown in **Fig. 8**. The total mechanism can be divided into the catalyst induction stage and the main catalysis stage. In the catalyst induction stage, H_2 reduces the monochromate and polychromate to form the active Cr(III) species and releases H_2O. These active Cr(III) sites can be reoxidized to produce monochromate and polychromate, releasing CO as the product.

In the main catalysis stage, the active Cr(III) sites generated from the reduction of Cr(VI) can excite the existed original Cr(III) and ZrO_2, adsorbing H_2 to form Cr-H and Zr-H, as detected by the In situ Raman experiments. At the same time, ZrO_2 adsorbs

CO_2 strongly, as shown by the CO_2 TPD results. Subsequently, the adsorbed H_2 and CO_2 react with each other and release the products: CO and H_2O.

These two stages occur simultaneously for the RWGS reaction with C-Cr/ZrO_2 as the catalyst. The catalyst induction caused by the Cr(VI) species increases the catalysis by Cr(III) in the main stage. It has also been reported that Cr(VI) interacts with nearby Cr(III) species and the metal oxide support surfaces, consequently forming Cr(VI)-Cr(III) pair sites that promote the redox catalytic activity of chromia[31]. This mechanism effectively explains the high catalytic activity of C-Cr/ZrO_2 because of the co-existence of Cr_2O_3, monochromate, and polychromate on the surface. The co-existence of Cr(III) and Cr(VI) species originated from the active Cr species because of the high dispersion when Cr(VI) was reduced and captured during the photoreduction by ZrO_2.

4. Conclusions

In this study, a high-performance catalyst for the RWGS reaction, Cr/ZrO_2, was obtained by a simple photoreduction process. The Cr(VI) in solution was photoreduced by ZrO_2 under UV light irradiation and immobilized to form a Cr/ZrO_2 composite. The obtained 1wt%Cr/ZrO_2 composite after calcination can effectively catalyze the RWGS reaction with 100% CO selectivity from 400 to 800 °C, reaching the thermodynamic limit at 600 °C and 38.34% CO yield. The stability of this 1wt%Cr/ZrO_2 catalyst was excellent, showing no significant performance decay after 72 h continuous operation at 500 °C.

The highly dispersed Cr species on the ZrO_2 surface resulting from the photoreduction process were the key species affecting the catalytic performance for the RWGS reaction. The photodeposited Cr(0) and Cr(III) were easily oxidized to form a multivalent mixture of Cr(III) and Cr(VI). The formed Cr(VI)-Cr(III) pair sites effectively promote the redox catalytic activity of chromia. Metal hydrides were determined to be the key intermediates in the RWGS reaction with Cr/ZrO_2 as catalyst, and the valence cycling of the Cr(VI)-Cr(III) pair sites caused by hydrogen reduction and CO_2 oxidization improves the catalytic activity.

This work has not only resulted in the development of a promising RWGS catalyst for CO_2 emission reduction and utilization but also provides an attractive strategy to treat Cr-containing wastewater and recover a useful by-product.

Acknowledgements

This work was supported by the National Natural Science Foundation of China (No. 21676168 & No. 21476146) and the Outstanding Young Scholar Fund of Sichuan University (No. 2015SCU04B06)

References

[1] R.W. Dorner, D.R. Hardy, F.W. Williams, H.D. Willauer, Energ Environ Sci.3 (2010) 884-890.
[2] B. Dai, G. Zhou, S. Ge, H. Xie, Z. Jiao, G. Zhang, K. Xiong, Can. J. Chem. Eng. 95 (2017).
[3] S.W. Park, O.S. Joo, K.D. Jung, H. Kim, S.H. Han, Appl. Catal., A. 211 (2001) 81-90.
[4] G. Centi, S. Perathoner, Catal. Today. 148 (2009) 191-205.
[5] S.S. Kim, H.H. Lee, S.C. Hong, Appl. Catal., A. 423-424 (2012) 100-107.
[6] L.C. Wang, M.T. Khazaneh, D. Widmann, R.J. Behm, J. Catal. 302 (2013) 20-30.
[7] M.R. Gogate, R.J. Davis, Catal. Commun. 11 (2010) 901-906.
[8] D.J. Pettigrew, D.L. Trimm, N.W. Cant, Catal. Lett. 28 (1994) 313-319.
[9] C.S. Chen, W.H. Cheng, S.S. Lin, Appl. Catal., A. 238 (2003) 55-67.
[10] B. Lu, K. Kawamoto, Mater. Res. Bull. 53 (2014) 70-78.
[11] Abolfazl, Gharibi, Kharaji, Ahmad, Shariati, Mohammad, Takassi, Chin. J. Chem. Eng. 21 (2013) 1007-1014.
[12] W. Wang, Y. Zhang, Z. Wang, J.M. Yan, Q. Ge, C.J. Liu, Catal. Today. 259 (2016) 402-408.
[13] K. Takehira, Y. Ohishi, T. Shishido, T. Kawabata, K. Takaki, Q. Zhang, Y. Wang, J. Catal. 224 (2004) 404-416.
[14] A. Mamedov, C. Rea, X. Zhang, J. Salazar, Low temperature methods for hydrogenation of CO_2 for production of syngas compositions with low H_2/CO ratios:, WO 2017074843 A1[P].2017.
[15] S.W. Park, O.S. Joo, K.D. Jung, H. Kim, S.H. Han, Korean J. Chem. Eng. 17 (2000) 719-722.
[16] ZHANG, QingHong, GAO, Lian, Huaxue Xuebao. 63 (2005) 65-70.
[17] C.T. Dinh, T.D. Nguyen, F. Kleitz, T.O. Do, ACS Appl. Mater. Interfaces. 3 (2011) 2228-2234.
[18] S.C. Chan, M.A. Barteau, Langmuir. 21 (2005) 5588.
[19] J.K. Yang, S.M. Lee, Chemosphere. 63 (2006) 1677-1684.
[20] Z. Jin, Y.X. Zhang, F.L. Meng, Y. Jia, T. Luo, X.Y. Yu, J. Wang, J.H. Liu, X.J. Huang, J. Hazard. Mater. 276 (2014) 400-407.
[21] Y. Xu, M.A.A. Schoonen, Am. Mineral. 85 (2000) 543-556.
[22] M. Roy, S. Ghosh, M.K. Naskar, Mater. Chem. Phys. 159 (2015) 101-106.
[23] E. Desimoni, C. Malitesta, P.G. Zambonin, J.C. Rivière, Surf. Interface Anal. 13 (1988) 173-179.
[24] C. Sleigh, A.P. Pijpers, A. Jaspers, B. Coussens, R.J. Meier, J. Electron Spectrosc. Relat. Phenom. 77 (1996) 41-57.
[25] G.C. Allen, M.T. Curtis, A.J. Hooper, P.M. Tucker, J. Chem. Soc., Dalton Trans. 13 (1973) 1675-1683.
[26] N. Anacleto, O. Ostrovski, Metall. Trans. B. 35 (2004) 609-615.
[27] G. Bai, H. Dai, Y. Liu, K. Ji, X. Li, S. Xie, Catal. Commun. 36 (2013) 43-47.
[28] D. Michel, M.P.Y. Jorba, R. Collongues, J. Raman Spectrosc. 5 (1976) 163-180.

[29]T.V. Malleswara Rao, G. Deo, J.M. Jehng, I.E. Wachs, Langmuir. 20 (2004) 7159.
[30]G. Busca, V. Lorenzelli, Mater. Chem.7 (1982) 89-126.
[31]R.B. Fahim, M.I. Zaki, N.E. Fouad, M. Abdel-Khalik, N. Sheppard, Appl. Catal., A. 265 (2004) 229-235.

Figure Captions

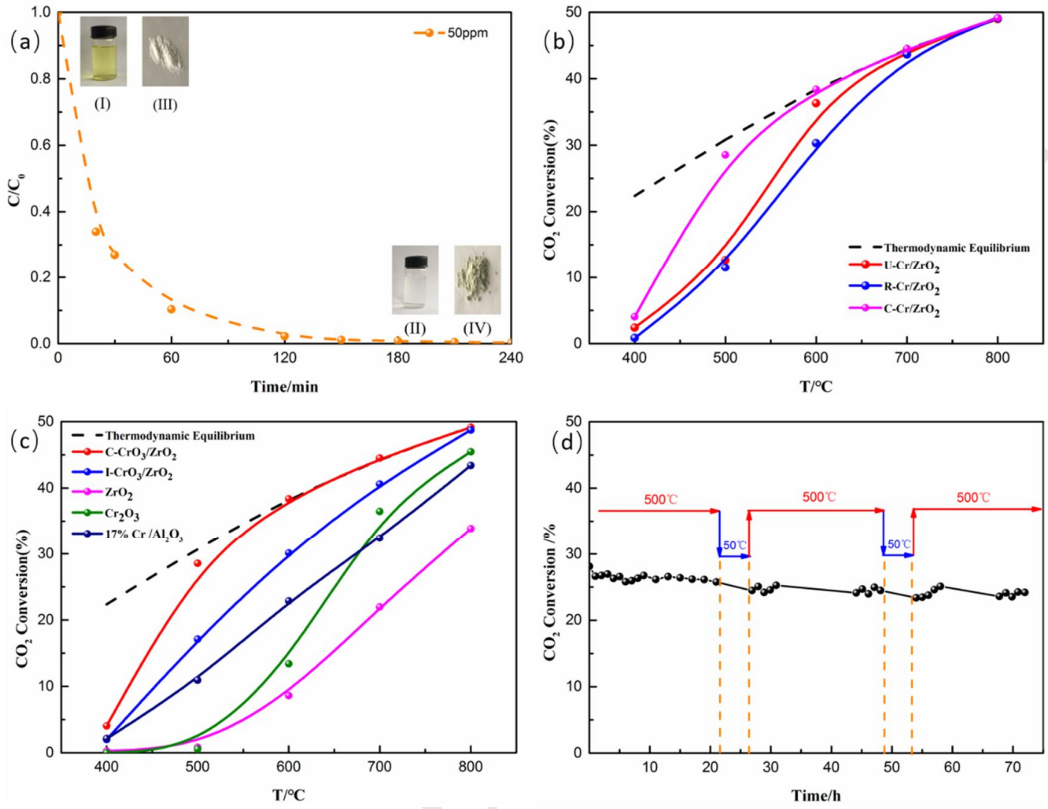

Fig. 1. The changes of Cr(IV) concentration, $K_2Cr_2O_7$ and ZrO_2 before and degradation, the RWGS with different types Cr/ZrO_2 ,17%Cr/Al_2O_3,pure ZrO_2 and Cr_2O_3 as catalysts: a) The Cr(IV) concentration detected by ICP during the degradation , I and II: $K_2Cr_2O_7$ before and after degradation; III and IV: ZrO_2 before and after degradation; b) The activities of U-Cr/ZrO_2,C-Cr/ZrO_2 and R-Cr/ZrO_2 and thermodynamic equilibrium of RWGS with CO_2:H_2=1:1,GSHV=22000 ml/(g •h); c) the activities of C-Cr/ZrO_2, I-Cr/ZrO_2, ZrO_2,Cr_2O_3,17%Cr/Al_2O_3 and thermodynamic equilibrium of RWGS with CO_2:H_2=1:1, 0.1Mpa ,GSHV=22000 ml/(g •h); d) The stability of C-Cr/ZrO_2 assessed at 500°C, 0.1Mpa, CO_2:H_2=1:1, and GHSV=22000mL/(g •h), intendedly shut down and restarted up twice, 72 hours continuous operation.

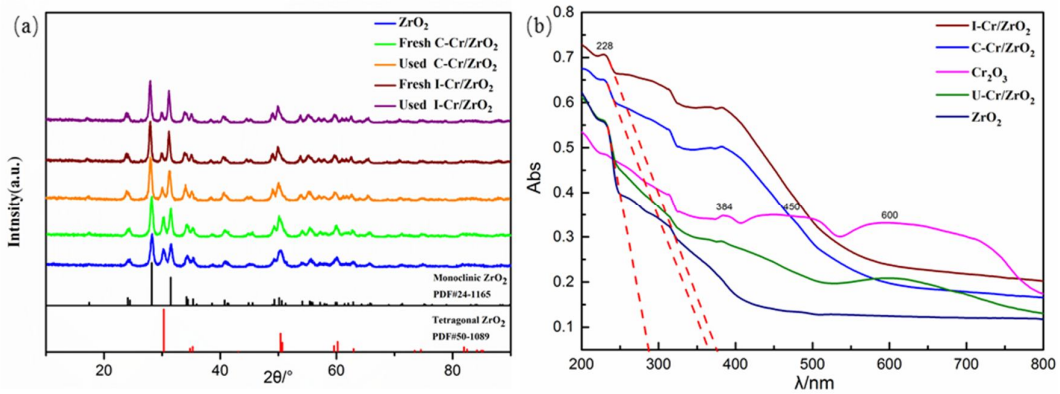

Fig. 2. Characterization of pure ZrO_2, pure Cr_2O_3, I-Cr/ZrO_2 C-Cr/ZrO_2, U-Cr/ZrO_2: a) XRD of pure ZrO_2, fresh and used of I-Cr/ZrO_2 and C-Cr/ZrO_2; b) UV-vis of pure ZrO_2, pure Cr_2O_3, I-Cr/ZrO_2 C-Cr/ZrO_2 U-Cr/ZrO_2.

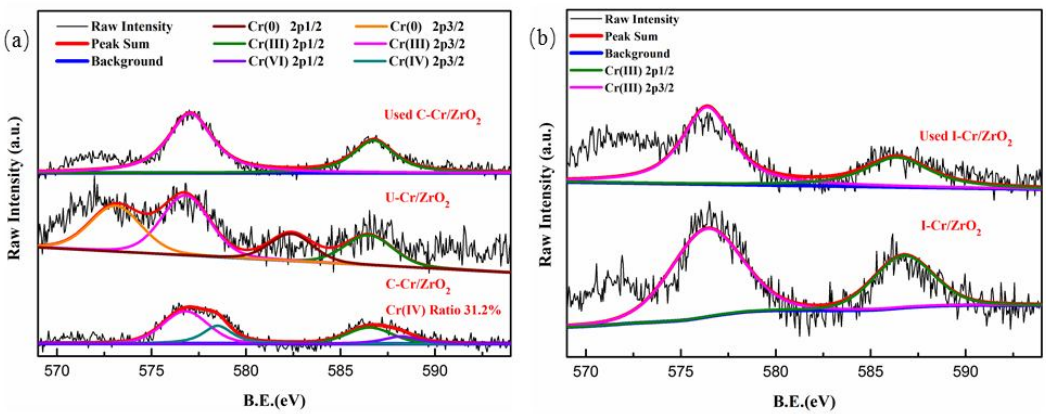

Fig. 3. XPS of U-Cr/ZrO_2, fresh and used of I-Cr/ZrO_2 C-Cr/ZrO_2: a) XPS of U-Cr/ZrO_2, C-Cr/ZrO_2 and used C-Cr/ZrO_2; b) XPS of I-Cr/ZrO_2 before and after reaction.

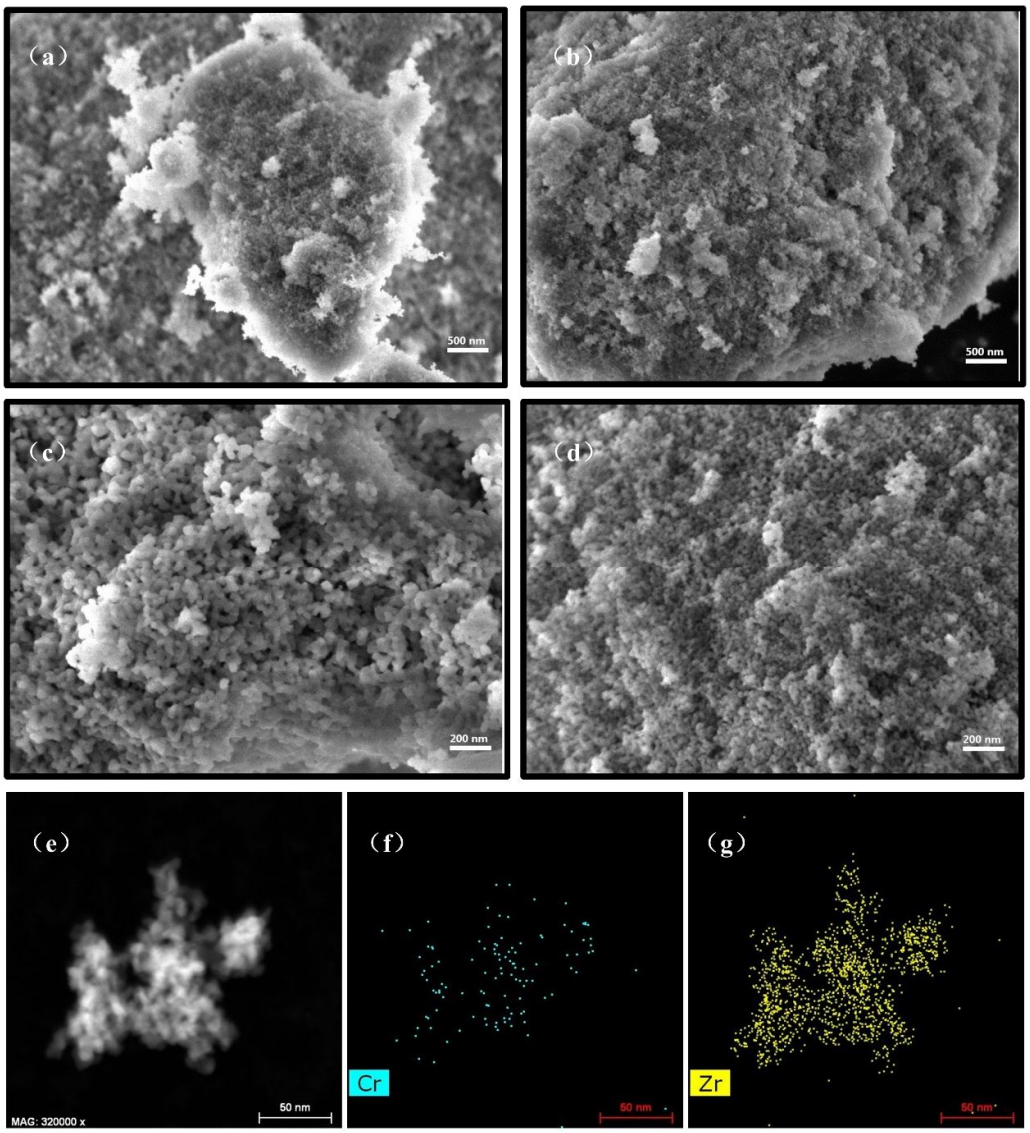

Fig. 4. SEM of fresh and used of I-Cr/ZrO_2 and C-Cr/ZrO_2: a) SEM of I-Cr/ZrO_2 before reaction; b) SEM of C-Cr/ZrO_2 before reaction; c) SEM of I-Cr/ZrO_2 after reaction; d) SEM of C-Cr/ZrO_2 after reaction; e-g) TEM mapping of C-Cr/ZrO_2

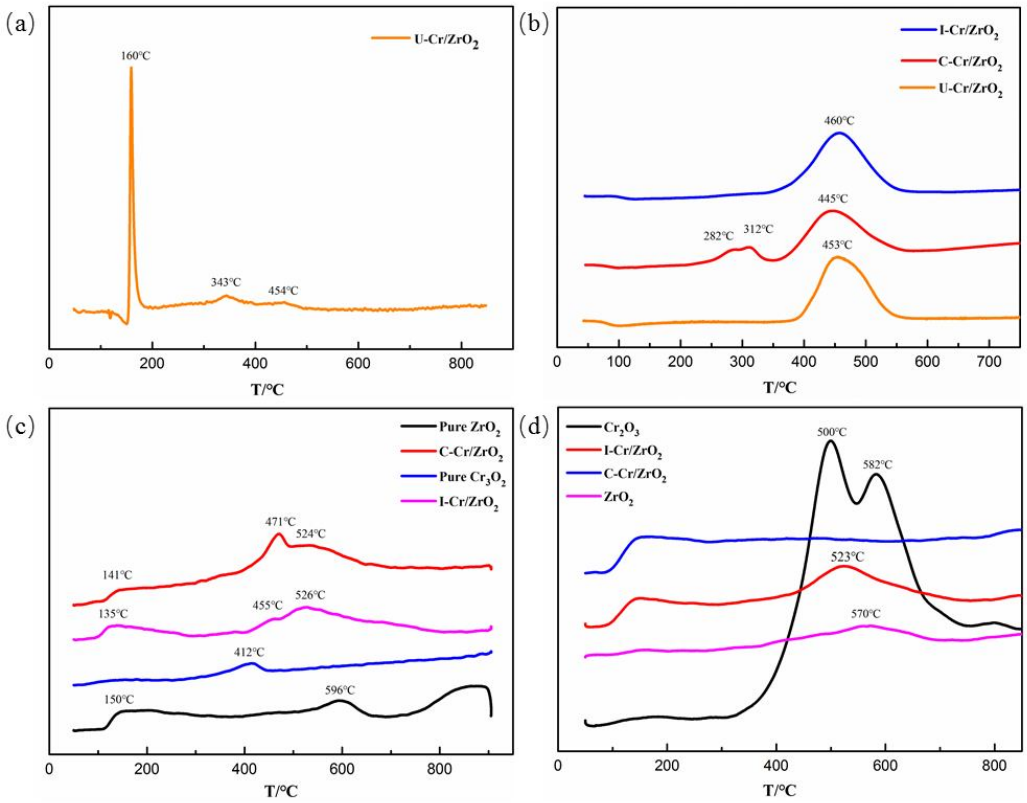

Fig. 5. TPX (X=O, R, D) of I-Cr/ZrO_2, C-Cr/ZrO_2, U-Cr/ZrO_2, pure ZrO_2 and pure Cr_2O_3: a) TPO of U-Cr/ZrO_2; b) TPR of C-Cr/ZrO_2, I-Cr/ZrO_2, U-Cr/ZrO_2; c) CO_2 TPD of I-Cr/ZrO_2, C-Cr/ZrO_2, pure ZrO_2 and pure Cr_2O_3; d) CO TPD of I-Cr/ZrO_2, C-Cr/ZrO_2, pure ZrO_2 and pure Cr_2O_3.

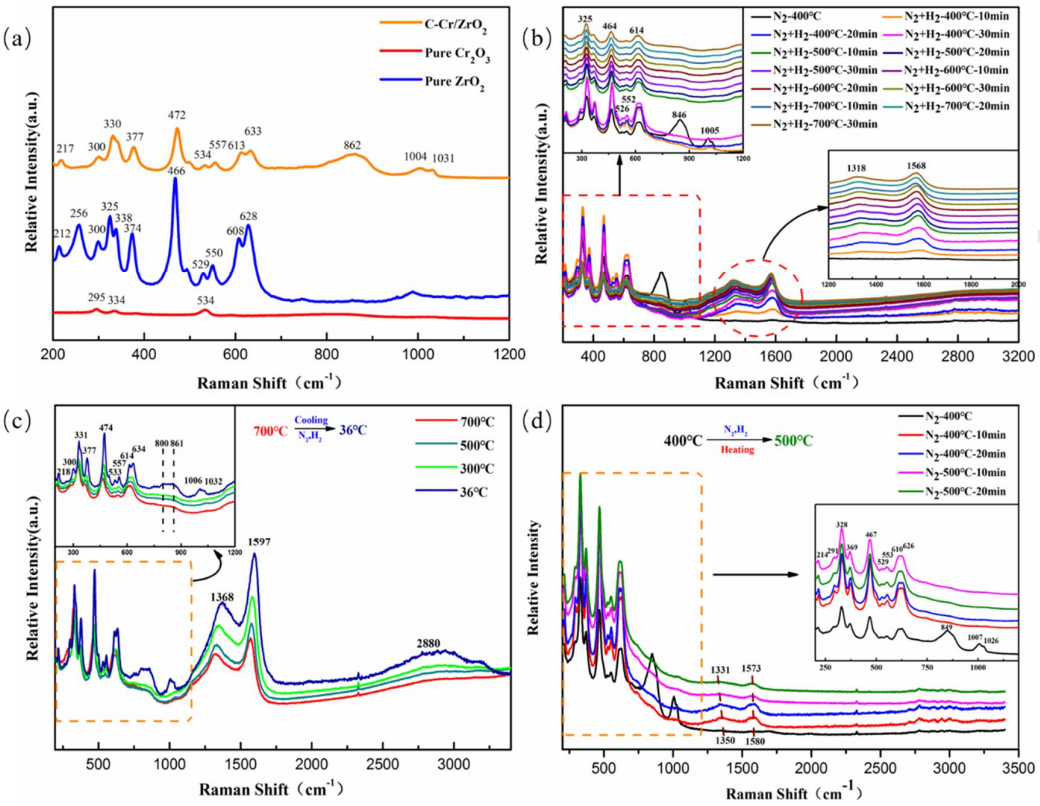

Fig. 6. In-Situ Raman Test of C-Cr/ZrO_2： a) Raman Test of C-Cr/ZrO_2, pure ZrO_2 and pure Cr_2O_3; b) In-Situ Raman Test of C-Cr/ZrO_2 with N_2 30ml/min, H_2 3ml/min and 0.1Mpa, from 400℃ to 700℃; c) In-Situ Raman Test of C-Cr/ZrO_2 with N_2 30ml/min, H_2 3ml/min and 0.1Mpa, cooling from 700℃ to 36℃; d) In-Situ Raman Test of C-Cr/ZrO_2 with N_2 30ml/min, H2 3ml/min and 0.1Mpa, heating from 400℃ to 500℃.

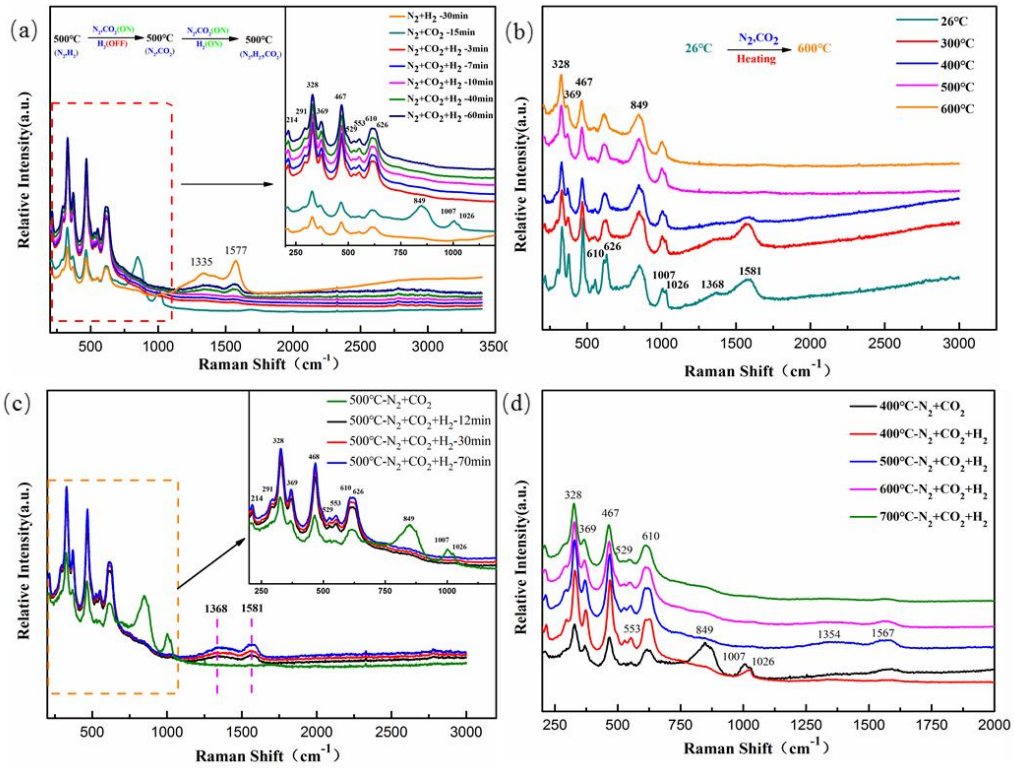

Fig. 7. In-Situ Raman Test of C-Cr/ZrO_2: a) In-Situ Raman Test of C-Cr/ZrO_2 with N_2 30ml/min, switch of CO_2 or H_2 for both 3ml/min and 0.1Mpa, at 500□; b) Raman Test of C-Cr/ZrO_2 with N_2 30ml/min, CO_2 3ml/min and 0.1Mpa, from 26□ to 600□; c) In-Situ Raman Test of C-Cr/ZrO_2 with N_2 30ml/min, H_2 3ml/min, CO_2 3ml/min and 0.1Mpa, at 500□; d) In-Situ Raman Test of C-Cr/ZrO_2 with N_2 30ml/min, H_2 3ml/min, CO_2 3ml/min and 0.1Mpa, cooling from 400□ to 700□.

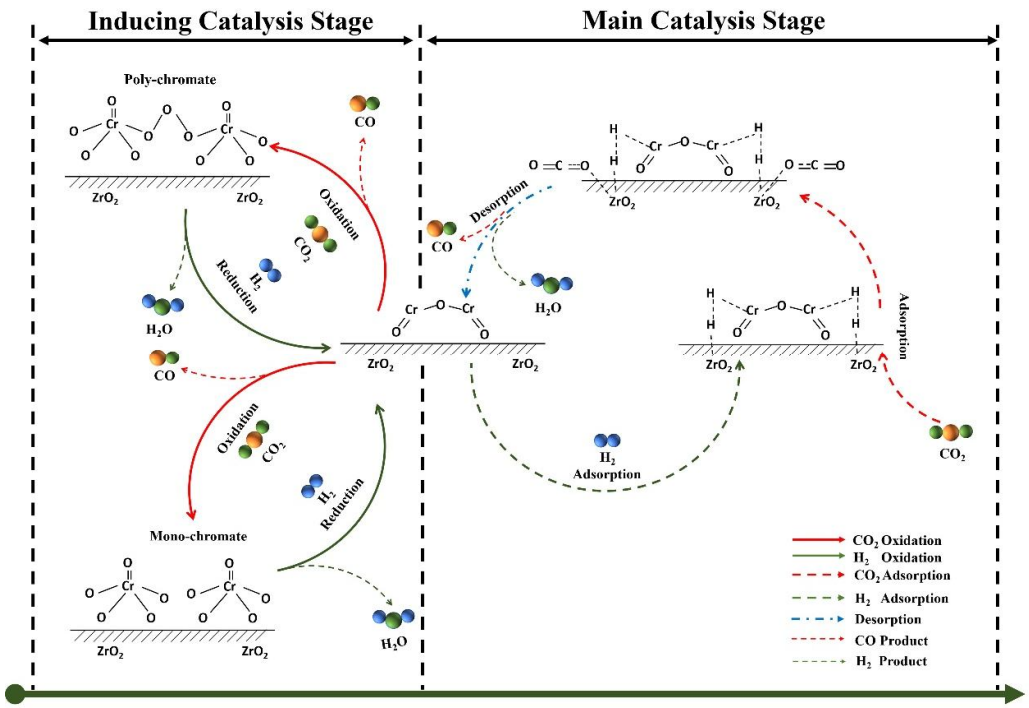

Fig. 8. Sketch map of mechanism of RWSG at C-Cr/ZrO_2.

Table 1 BET results of pure ZrO_2, fresh and used C-Cr/ZrO_2 and I-Cr/ZrO_2

	BET/(m^2/g)	Pore Size/nm	Pore Volume/(cm^3/g)
Pure ZrO_2	62	16	0.24
Fresh C-Cr/ZrO_2	45	18	0.20
Fresh I-Cr/ZrO_2	51	18	0.22
Used C-Cr/ZrO_2	18	37	0.13
Used I-Cr/ZrO_2	20	39	0.16

Table 2 Amount of chemical adsorption for CO_2 and CO of pure ZrO_2, Cr_2O_3, C-Cr/ZrO_2 and I-Cr/ZrO_2

	Amount of Chemical Adsorption for CO_2/ (μmoL/g)	Amount of Chemical Adsorption for CO/ (μmoL/g)
ZrO_2	317.66	101.54
Cr_2O_3	34.95	843.10
C-Cr/ZrO_2	394.97	95.59
I-Cr/ZrO_2	328.32	331.41

HIGHLIGHTS：

1. Thermodynamic limit CO_2 conversion and 100% CO selectivity at 600℃ in RWGS with Cr/ZrO_2.

2. Excellent stability of photoreduced Cr/ZrO2 in 72 hours continuous operation at 500℃.

3. Co-existence of Cr(0) and Cr(III) in on ZrO_2 surface after photoreduction process.

4. Intermediate role of Cr(VI) in RWGS reaction with Cr/ZrO_2 as catalyst.

5. Possibility of recover Cr species in water as high performance catalyst for CO_2 utilization.